CrossMPT: Cross-attention Message-Passing Transformer for Error Correcting Codes

Anonymous authors
Paper under double-blind review

Abstract

Error correcting codes (ECCs) are indispensable for reliable transmission in communication systems. The recent advancements in deep learning have catalyzed the exploration of ECC decoders based on neural networks. Among these, transformer-based neural decoders have achieved state-of-the-art decoding performance. In this paper, we propose a novel Cross-attention Message-Passing Transformer (CrossMPT), which shares key operational principles with conventional message-passing decoders. While conventional transformer-based decoders employ self-attention mechanism without distinguishing between the types of input vectors (i.e., magnitude and syndrome vectors), CrossMPT updates the two types of input vectors separately and iteratively using two masked cross-attention blocks. The mask matrices are determined by the code's parity-check matrix, which explicitly captures the irrelevant relationship between two input vectors. Our experimental results show that CrossMPT significantly outperforms existing neural network-based decoders for various code classes. Notably, CrossMPT achieves this decoding performance improvement, while significantly reducing the memory usage, complexity, inference time, and training time.

1 Introduction

The fundamental objective of digital communication systems is to reliably transmit information from source to destination through noisy channels. Error correcting codes (ECCs) are crucial for ensuring the integrity of transmitted data in digital communication systems. The advancements in deep learning across diverse tasks, such as natural language processing (NLP), image classification, or object detection (Devlin et al., 2019; He et al., 2016; Girshick et al., 2014; Carion et al., 2020), have motivated the application of deep learning techniques to ECC decoders. This has led to the development of neural decoders (Kim et al., 2018; 2020; Nachmani et al., 2016; 2018; Dai et al., 2021; Lugosch & Gross, 2017). The key aim of these neural decoders is to improve decoding performance by overcoming limitations of the conventional decoders such as belief propagation (BP) (Richardson & Urbanke, 2001) or min-sum (MS) (Fossorier et al., 1999) decoders.

Among neural decoders, model-free neural decoders employ an arbitrary neural network architecture (e.g., deep neural networks (Gruber et al., 2017), recurrent neural networks (Bennatan et al., 2018) and transformers (Choukroun & Wolf, 2022a; 2023; Park et al., 2023; Choukroun & Wolf, 2024a;b)) as the ECC decoder, without relying on prior knowledge of specific decoding algorithms. Since model-free neural decoders are not based on specific decoding algorithms, their training is prone to overfitting, largely due to the exponentially large number of codewords (Bennatan et al., 2018). To circumvent overfitting, these neural decoders incorporate a preprocessing step where the magnitude and syndrome vectors from the received codeword are concatenated and used as inputs. The preprocessing step is essential for integrating an effective network architecture for the ECC decoder without an overfitting issue (Bennatan et al., 2018). For example, transformer-based ECC decoders (Choukroun & Wolf, 2022a; 2023; Park et al., 2023; Choukroun & Wolf, 2024a;b) achieve state-of-the-art decoding performance. However, two important questions have not been addressed: 1) how to effectively manage the two distinct input vectors (magnitude and syndrome), and 2) how to design an efficient transformer-based decoder architecture.

Conventional transformer-based ECC decoders, initially proposed as Error Correction Code Transformer (ECCT) (Choukroun & Wolf, 2022a; 2023; Park et al., 2023; Choukroun & Wolf, 2024a;b), receive the concatenated magnitude and syndrome embeddings as a single input and utilize self-attention blocks, without a distinct process for handling the two different types of vectors. In contrast, our approach treats the magnitude and syndrome as *multimodal data*, recognizing their distinct informational characteristics. The *real-valued* magnitude vector contains the reliabilities of all bit positions, while the *binary* syndrome vector conveys the information of erroneous bit positions. This deliberate separation necessitates the development of a novel architecture, specifically designed to effectively update these separated magnitude and syndrome embeddings, thereby significantly improving decoding performance.

In this paper, we introduce a novel Cross-attention Message-Passing Transformer (CrossMPT) for ECC decoding. CrossMPT processes the magnitude and syndrome separately to effectively utilize their distinct informational properties. It employs two *cross-attention blocks* to iteratively update the magnitude and syndrome embeddings. Initially, the magnitude embedding is encoded into the *query*, while the syndrome embedding is encoded into *key* and *value*. The first cross-attention block utilizes this configuration in its attention mechanism to update the magnitude embedding component. This procedure is reciprocated for the syndrome embedding, which is encoded into the query, while the magnitude embedding is encoded into the key and value. This configuration enables the second cross-attention block to update the syndrome vector component. These two masked cross-attention blocks iteratively collaborate to refine the magnitude and syndrome embeddings as in the message-passing algorithm (Richardson & Urbanke, 2001).

To facilitate training, CrossMPT employs a mask matrix for each cross-attention block. The first cross-attention block uses the transpose of the parity check matrix (PCM) H^T as its mask matrix with the magnitude embedding as the query. In the second cross-attention block, the PCM $H^\top$ itself is applied as the mask matrix, with the syndrome embedding acting as the query. This strategy leverages the PCM's inherent representation of the 'magnitude-syndrome' relationship, effectively aligning with the architecture's objectives. Moreover, the combined size of the two attention maps of CrossMPT is at most half that of the attention map of the conventional transformer-decoder, leading to significantly reduced memory usage. This reduction enables efficient learning and decoding of longer codes, which previous approaches (concatenating magnitude and syndrome embeddings) are unable to achieve due to high memory usage and computational complexity. To our knowledge, CrossMPT is the first architecture to integrate an iterative message-passing framework with a cross-attention-based transformer architecture.

Experimental results show that CrossMPT consistently outperforms the original ECCT across various code classes. Leveraging its shared operational principles with the message-passing algorithm, CrossMPT demonstrates particularly improved decoding performance, especially in low-density parity-check (LDPC) codes. Notably, we also demonstrate that CrossMPT closely approaches the maximum likelihood decoding performance on short codes. In addition to its enhanced decoding performance, CrossMPT significantly reduces the computational complexity (e.g., floating point operations (FLOPs), training time, and inference time) of the decoder layer compared to the original ECCT. Given that the decoder layer constitutes a substantial portion of the total computational cost, this reduction leads to a significant decrease in overall computational complexity.

2 Related Works

In the field of neural network-based ECC decoders, there are two primary categories: the model-based decoder and the model-free decoder. First, model-based decoders are constructed based on the conventional decoding methods (e.g., BP decoder and MS decoder). They map the iterative decoding process of the conventional decoding methods into neural networks and train the network weights accordingly. To improve performance over the standard BP decoder, the recurrent neural network was employed for the decoding of BCH codes (Nachmani et al., 2018). Several recent studies showed that neural network-based BP and MS decoders outperform the conventional decoding algorithms over various code types (Dai et al., 2021; Kwak et al., 2023; Lugosch & Gross, 2017; Nachmani & Wolf, 2019; 2021; Kwak et al., 2022; Buchberger et al., 2021). However, model-based neural decoders may encounter performance limitations due to their restrictive model architectures, which are closely tied to underlying decoding methods.

Unlike model-based decoders, which are constrained by the limitations of their underlying algorithms (e.g., BP), model-free neural decoders use arbitrary architectures to learn decoding without

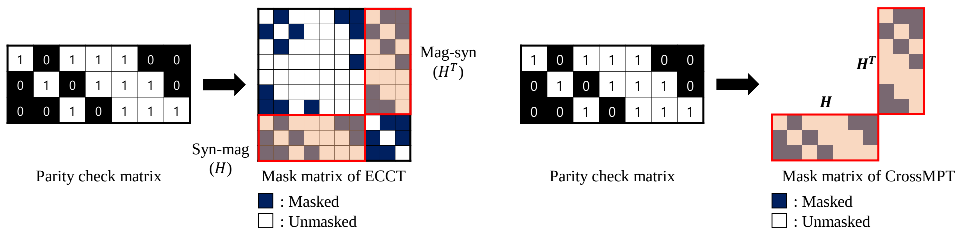

(a) ECCT (Choukroun & Wolf, 2022a) (b) CrossMPT

Figure 1: The PCM and the mask matrices of ECCT and CrossMPT

such restrictions. While early approaches (Gruber et al., 2017; Cammerer et al., 2017; Kim et al., 2018) employed fully connected networks, they faced overfitting challenges during training. Subsequently, the introduction of a preprocessing step utilizing the magnitude and syndrome vectors of the received codeword to learn multiplicative noise has been pivotal in enabling model-free decoders to address the overfitting issue (Bennatan et al., 2018). Then, ECCT (Choukroun & Wolf, 2022a) first employed the transformer architecture using the same preprocessing step and demonstrated that the transformer-based decoder outperforms existing decoders including model-based neural decoders. Building on the ECCT framework, denoising diffusion error correction codes (Choukroun & Wolf, 2023) interpreted the iterative decoding process as a diffusion process and incorporated a diffusion model to train the original ECCT. Recently, double-masked ECCT (Park et al., 2023) utilized two different PCMs for the same linear code to capture the diverse multilateral relationships of the magnitude and syndrome bits and improve the decoding performance. Notably, transformer-based decoders outperform model-based neural decoders and serve as universal decoders capable of decoding arbitrary code classes with a unified architecture.

Furthermore, employing cross-attention mechanisms in architecture has enhanced performance across various domains. In NLP, the transformer decoder (Vaswani et al., 2017) adopted the cross-attention modules. In vision, CrossViT (Chen et al., 2021) utilized cross-attention for improved image classification. For text-based image generation, latent diffusion models (Rombach et al., 2022) integrated cross-attention layers into the model architecture, enabling diffusion models to become powerful and flexible generators. These works demonstrate the versatility of cross-attention, inspiring its application to ECC decoding.

3 BACKGROUND

3.1 ERROR CORRECTING CODES

Let C be a linear block code, which is defined by a generator matrix G of size $k \times n$ and a parity check matrix H of size $(n-k) \times n$. They satisfy $GH^\top = 0$ over $\{0,1\}$ with modulo 2 addition. A codeword $x \in C \subset \{0,1\}^n$ is encoded by multiplying message m with the generator matrix G (i.e., $x = mG$). Let x_s be the binary phase shift keying (BPSK) modulated signal of x and let y be the output of a noisy channel for input x_s. We assume the additive white Gaussian noise (AWGN) channel and the channel output can be represented by $y = x_s + z$, where $z \sim N(0, \sigma^2)$. The objective of the decoder ($f : \mathbb{R}^n \to \mathbb{R}^n$) is to recover the transmitted codeword x by correcting errors. When y is received, the decoder first determines whether the received signal is corrupted or not by checking the syndrome $s(y) = Hy_b$, where $y_b = \text{bin}(\text{sign}(y))$ is the demodulated signal of y. Here, $\text{sign}(a)$ represents $+1$ if $a \geq 0$ and -1 otherwise and $\text{bin}(-1) = 1, \text{bin}(+1) = 0$. If $s(y)$ is a non-zero vector, it is detected that y is corrupted during the transmission, and the decoder initiates the error correction process.

3.2 ERROR CORRECTION CODE TRANSFORMER

ECCT is the first approach to present a model-free decoder with the transformer architecture. ECCT outperforms other neural BP-based decoders by employing the masked self-attention mechanism,

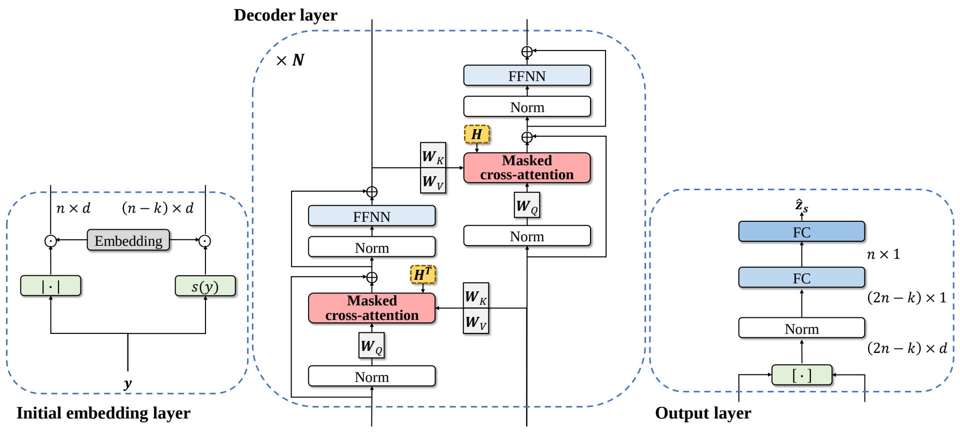

Figure 2: Architecture of CrossMPT.

whose mask matrix is determined by the code's PCM (Choukroun & Wolf, 2022a). The first issue that needs to be addressed when training transformer-based decoders is the overfitting. In (Bennatan et al., 2018), the overfitting issue in model-free neural decoders is described as a poor generalization to untrained new codewords due to the exponentially large number of codewords. However, it has been resolved by a preprocessing technique that facilitates a syndrome-based decoding (Bennatan et al., 2018). It has been theoretically proven that, with this preprocessing step, the decoder's performance is invariant to the specific codewords in the training set (Bennatan et al., 2018).

As in (Bennatan et al., 2018), the preprocessing step of ECCT utilizes the magnitude and syndrome vectors to train multiplicative noise $\tilde{z}_s$, which is defined by

$$y = x_s + z = x_s \tilde{z}_s. \tag{1}$$

ECCT aims to estimate the multiplicative noise in (1), i.e., $f(y) = \hat{z}_s$. Then, the estimation of x is $\hat{x} = \text{bin}(\text{sign}(yf(y)))$. If the multiplicative noise is correctly estimated such that $\text{sign}(\tilde{z}_s) = \text{sign}(\hat{z}_s)$, then $\hat{x}$ can be computed as:

$$\hat{x} = \text{bin}(\text{sign}(yf(y))) = \text{bin}(\text{sign}(x_s \tilde{z}_s \hat{z}_s)) = \text{bin}(\text{sign}(x_s)) = x.$$

ECCT employs a masked self-attention module to train the transformer architecture, where the input embedding is the concatenation of the embedded magnitude and syndrome vector of y. As shown in Figure 1, the mask matrice of ECCT should clearly distinguish between necessary (unmasked) and unnecessary (masked) pairwise relationships among magnitude-magnitude, magnitude-syndrome, and syndrome-syndrome bit relations. In ECCT, the syndrome-syndrome part was only unmasked for self-relations, while the magnitude-syndrome part was unmasked based on the connections defined by the parity-check matrix (PCM). The magnitude-magnitude part, however, was unmasked for bit pairs connected at depth 2 (see Algorithm 1 in Choukroun & Wolf (2022a)). While the masking of magnitude-syndrome relations is intuitive, as it directly uses PCM, determining the relationships among magnitude themselves is not directly derivable from the PCM. Therefore, the algorithm for masking magnitude-magnitude part is neither straightforward nor unique. In Figure 1, the white areas indicate unmasked positions (require the attention calculation) whereas the blue areas represent masked positions (omit the attention calculation). As the proportion of blue increases, the attention matrix becomes sparser and more cost-efficient.

4 Cross-attention Message-Passing Transformer

In this section, we present the operational mechanism and architecture of CrossMPT. CrossMPT handles the magnitude and syndrome embeddings separately, applying a cross-attention mechanism to effectively capture their distinct information. It shares its core principles with message passing decoding algorithm for decoding linear codes, where the magnitude and syndrome embeddings of the received codewords are iteratively updated. The overall architecture is illustrated in Figure 2.

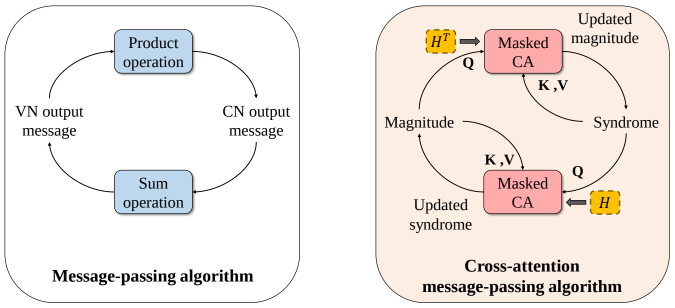

Figure 3: Conceptual comparison of the sum-product message-passing algorithm and the proposed cross-attention (CA) message-passing algorithm.

4.1 Cross-attention Message-passing Transformer

One cross-attention block updates the magnitude embedding by using it as a query and updates them with key and value, generated from the syndrome embedding. Given this configuration, the attention map has the size $n \times (n-k)$, effectively representing the 'magnitude-syndrome' relation. To reflect this relationship, we employ the transpose of the PCM $H^\top$ as the mask matrix. This is because the n rows of $H^\top$ correspond to the n bit positions, and its $n-k$ columns are associated with the parity check equations, directly linking to $|y|$ and $s(y)$, respectively. The other cross-attention block similarly use $s(y)$ is used as the query, while $|y|$ serves as both key and value. For this operation, we utilize the PCM H as the mask matrix.

This configuration of separately handling two distinct informational properties resembles the message-passing decoding algorithm for decoding linear codes. Message-passing algorithms such as the sum-product algorithm (Richardson & Urbanke, 2001) are widely used for decoding ECCs due to their outstanding decoding performance with low complexity. The message-passing algorithm operates by exchanging messages between variable nodes (VNs) and check nodes (CNs) over a Tanner (bipartite) graph (Richardson & Urbanke, 2001). In the Tanner graph, VNs convey information about the reliability of the received codeword, while CNs indicate the parity check equations. The edges between VNs and CNs represent the connections (relationships) between them. The message-passing decoder operates by exchanging messages between VNs and CNs via edges. The output messages of VNs and CNs are updated in an iterative manner.

Similar to the principles of message-passing algorithms, CrossMPT updates $|y|$ and $s(y)$ by allowing them to exchange messages with each other. Initially, we update $|y|$ by the masked cross-attention block, with $|y|$ as the query and $s(y)$ as both the key and value. The syndrome embedding is updated in the subsequent masked cross-attention block, utilizing the previously updated magnitude embedding. In this block, the syndrome embedding is used as the query, while the updated magnitude embedding serves as the key and value. The resulting output from this cross-attention block is the updated syndrome. CrossMPT iteratively updates both the magnitude and syndrome embeddings to identify the multiplicative noise accurately.

As a representative of the message-passing algorithm, Figure 3 depicts the sum-product algorithm and the cross-attention message-passing algorithm. In the sum-product algorithm, the VN output and CN output messages are iteratively updated using the sum and product operations. Similar to the sum-product algorithm, the magnitude and syndrome embeddings are iteratively updated using the masked cross-attention (Masked CA in the figure) blocks in CrossMPT. Note that H and $H^\top$ are utilized for the mask matrices for these cross-attention blocks, and Q, K, and V represent the query, key, and value of the cross-attention mechanism.

4.2 Model Architecture

In the initial embedding layer, we generate $|y| = (|y_1|, \dots, |y_n|)$ and $s(y) = (s(y)_1, \dots, s(y)_{n-k})$ from the received codeword, and project each element y_i and $s(y)_i$ into d dimension embedding row vectors M_i and S_i, respectively, as follows:

$$\begin{aligned} M_i &= |y_i| W_i, && \text{for } i = 1, \dots, n, \\ S_i &= s(y)_i W_{i+n}, && \text{for } i = 1, \dots, n-k, \end{aligned}$$

where $W_i \in \mathbb{R}^{1\times d}$ for $i = 1, \dots, 2n-k$ denote the trainable positional encoding vector.

These two embedded vectors are processed as separate input vectors in the following N decoding layers. Each decoding layer contains two cross-attention blocks, each consisting of a cross-attention module, a feed-forward neural network (FFNN), and a normalization layer.

In the first cross-attention module, the attention module updates the 'magnitude' embedding by using the syndrome. The query vector Q_1, key vector K_1, and value vector V_1 are assigned as follows:

$$Q_1 = MW_Q, K_1 = SW_K, V_1 = SW_V,$$

where $M = [M_1; \cdots; M_n] \in \mathbb{R}^{n\times d}$ and $S = [S_1; \cdots; S_{n-k}] \in \mathbb{R}^{(n-k)\times d}$ denote the magnitude embedding and the syndrome embedding, respectively, and W_Q, W_K, W_V denote the weight matrices of query, key, and value, respectively. This architecture is termed the 'cross-attention' message-passing transformer since the query corresponds to the magnitude embedding, while the key and value correspond to the syndrome embedding. Then, we employ the following scaled dot-product attention:

$$\text{Attention}(Q_1, K_1, V_1) = \text{softmax}\left(\frac{Q_1 K_1^\top + g(H^\top)}{\sqrt{d}}\right) V_1,$$

where $g(H^\top)$ is the mask matrix, and the function g is defined as

$$g(A)_{i,j} = \begin{cases} 0 & \text{if } A_{i,j} = 1, \\ -\infty & \text{if } A_{i,j} = 0. \end{cases} \tag{2}$$

This configuration results in an attention map of size $n \times (n-k)$, representing the 'magnitude-syndrome' relationship. Therefore, we use the transpose of the PCM $H^\top$ as a mask matrix since the n rows of $H^\top$ correspond to the n bit positions and the $n-k$ columns of $H^\top$ to the parity check equations, which are closely related to $|y|$ and $s(y)$, respectively. Finally, the output vector embodies a newly updated magnitude embedding M' by using the syndrome.

In the second cross-attention module, we update the 'syndrome' embedding with the updated M' corresponding to the magnitude. In other words, the input of the query becomes syndrome and the input of key and value becomes M'. We use the *shared weight vectors* W_Q, W_K, W_V as in the first cross-attention module, and query vector Q_2, key vector K_2, and value vector V_2 are defined as follows:

$$Q_2 = SW_Q, K_2 = M'W_K, V_2 = M'W_V.$$

Here, the syndrome and magnitude correspond the row and column of the attention map, respectively. Thus, we employ the mask matrix $g(H)$, whose masking positions are zeros in H. Then we apply the scaled dot-product attention and the resulting output vector conveys the updated syndrome. This output vector is utilized to further refine the magnitude embedding and this process is iteratively repeated across the N decoder layers.

Finally, these output vectors of the last decoder layer are concatenated and pass through a normalization layer and two fully connected (FC) layers. The first FC layer reduces the $(2n-k) \times d$ dimension embedding to a one-dimensional $2n-k$ vector, and the second FC layer further reduces the dimension from $2n-k$ into n. The final output provides an estimation of $\tilde{z}_s$. Since two cross-attention blocks of CrossMPT share the same weight matrices W_Q, W_K, W_V and all other layers, CrossMPT has the same number of parameters as the original ECCT.

The objective of the proposed decoder is to learn the multiplicative noise $\tilde{z}_s$ in (1) and reconstruct the original transmitted signal x. We can obtain the multiplicative noise by $\tilde{z}_s = \tilde{z}_s x_s^2 = y x_s$. Then, the target multiplicative noise for binary cross-entropy loss function is defined by $\tilde{z} = \text{bin}(\text{sign}(y x_s))$. Finally, the cross-entropy loss function for a received codeword y is defined by

$$\mathcal{L} = -\sum_{i=1}^{n} \left\{ \tilde{z}_i \log(\sigma(f(y))) + (1 - \tilde{z}_i) \log(1 - \sigma(f(y))) \right\}.$$

Table 1: Comparison of decoding performance at three different SNR values (4 dB, 5 dB, 6 dB) for BP decoder, Hyper BP decoder (Nachmani & Wolf, 2019), AR BP decoder (Nachmani & Wolf, 2021), ECCT (Choukroun & Wolf, 2022a), and the proposed CrossMPT. The results are measured by the negative natural logarithm of BER. The best results are highlighted in **bold**. Higher is better.

Architecture		BP-based decoders									Model-free decoders					
Codes	Parameter	BP			Hyp BP			AR BP			ECCT			CrossMPT		
		4	5	6	4	5	6	4	5	6	4	5	6	4	5	6
BCH	(31,16)	4.63	5.88	7.60	5.05	6.64	8.80	5.48	7.37	9.60	6.39	8.29	10.66	**6.98**	**9.25**	**12.48**
	(63,36)	4.03	5.42	7.26	4.29	5.91	8.01	4.57	6.39	8.92	4.86	6.65	9.10	**5.03**	**6.91**	**9.37**
	(63,45)	4.36	5.55	7.26	4.64	6.27	8.51	4.97	6.90	9.41	5.60	7.79	10.93	**5.90**	**8.20**	**11.62**
	(63,51)	4.5	5.82	7.42	4.8	6.44	8.58	5.17	7.16	9.53	5.66	7.89	11.01	**5.78**	**8.08**	**11.41**
Polar	(64,32)	4.26	5.38	6.50	4.59	6.10	7.69	5.57	7.43	9.82	6.99	9.44	12.32	**7.50**	**9.97**	**13.31**
	(64,48)	4.74	5.94	7.42	4.92	6.44	8.39	5.41	7.19	9.30	6.36	8.46	11.09	**6.51**	**8.70**	**11.31**
	(128,64)	4.1	5.11	6.15	4.52	6.12	8.25	4.84	6.78	9.3	5.92	8.64	12.18	**7.52**	**11.21**	**14.76**
	(128,86)	4.49	5.65	6.97	4.95	6.84	9.28	5.39	7.37	10.13	6.31	9.01	12.45	**7.51**	**10.83**	**15.24**
	(128,96)	4.61	5.79	7.08	4.94	6.76	9.09	5.27	7.44	10.2	6.31	9.12	12.47	**7.15**	**10.15**	**13.13**
LDPC	(49,24)	6.23	8.19	11.72	6.23	8.54	11.95	6.58	9.39	12.39	6.13	8.71	12.10	**6.68**	**9.52**	**13.19**
	(121,60)	4.82	7.21	10.87	5.22	8.29	13.00	5.22	8.31	13.07	5.17	8.31	13.30	**5.74**	**9.26**	**14.78**
	(121,70)	5.88	8.76	13.04	6.39	9.81	14.04	6.45	10.01	14.77	6.40	10.21	16.11	**7.06**	**11.39**	**17.52**
	(121,80)	6.66	9.82	13.98	6.95	10.68	15.80	7.22	11.03	15.90	7.41	11.51	16.44	**7.99**	**12.75**	**18.15**
MacKay	(96,48)	6.84	9.40	12.57	7.19	10.02	13.16	7.43	10.65	14.65	7.38	10.72	14.83	**7.97**	**11.77**	**15.52**
CCSDS	(128,64)	6.55	9.65	13.78	6.99	10.57	15.27	7.25	10.99	16.36	6.88	10.90	15.90	**7.68**	**11.88**	**17.50**
Turbo	(132,40)	N/A	N/A	N/A	N/A	N/A	N/A	N/A	N/A	N/A	4.74	6.54	9.06	**5.55**	**7.92**	**10.94**

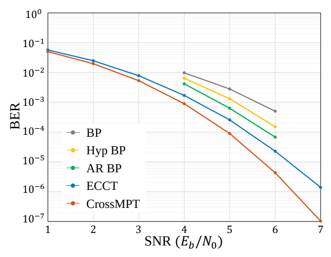

(a) $(31, 16)$ BCH code

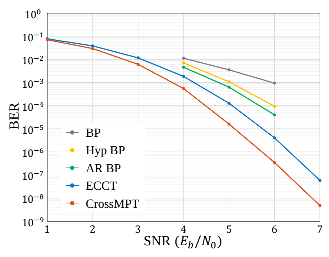

(b) $(128, 86)$ polar code

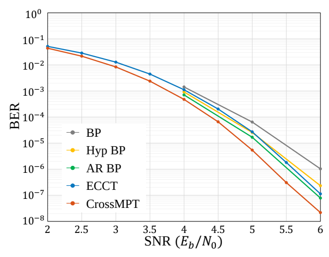

(c) $(128, 64)$ CCSDS

Figure 4: The BER performance of various decoders (BP, Hyp BP, AR BP, ECCT) and CrossMPT.

To ensure a fair comparison between CrossMPT and ECCT, we adopt the same training setup used in the previous work (Choukroun & Wolf, 2022a). We use the Adam optimizer (Kingma & Ba, 2015) and conduct 1000 epochs. Each epoch consists of 1000 minibatches, where each minibatch is composed of 128 samples. All simulations were conducted using NVIDIA GeForce RTX 3090 GPU and AMD Ryzen 9 5950X 16-Core Processor CPU. The training sample y is generated by $y = x_s + z$, where x_s is the all-zero codeword and the AWGN channel noise z is from an SNR (E_b/N_0) range of 3 dB to 7 dB. The learning rate is initially set to 10^{-4} and gradually reduced to 5×10^{-7} following a cosine decay scheduler.

5 Experimental Results

In this section, we compare the proposed CrossMPT with the original ECCT across various code classes. Our experimental results do not include a comparison with the works of (Choukroun & Wolf, 2024a;b), as they have different objectives, such as generalizing the decoder to unseen codes (Choukroun & Wolf, 2024a) or jointly training the encoder and decoder (Choukroun & Wolf, 2024b). It is worth mentioning that our cross-attention architecture and the schemes of (Choukroun & Wolf, 2024a;b) are orthogonal methods, and combining them could present a promising direction for future research.

To verify the efficacy of CrossMPT, we train it for BCH codes, polar codes, turbo codes, and LDPC codes (including MacKay and CCSDS codes) and evaluate the bit error rate (BER) performance.

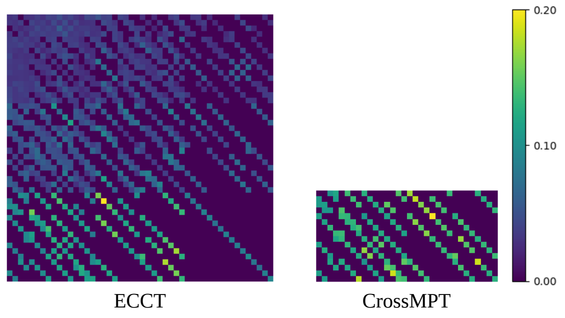

Figure 5: The average attention scores of all $N = 6$ layers for ECCT and CrossMPT.

All PCMs are taken from (Helmling et al., 2019). The implementation of the original ECCT is taken from (Choukroun & Wolf, 2022b). For the testing, we collect at least 500 frame errors at each signal-to-noise ratio (SNR) value with random codewords. Table 1 compares the decoding performance of CrossMPT with the BP decoder, BP-based neural decoders (Nachmani & Wolf, 2019; 2021), and ECCT (Choukroun & Wolf, 2022a). The results of the BP-based decoders in Table 1 are obtained for 50 iterations. The results for both the proposed CrossMPT and ECCT, which are model-free decoders, are obtained with $N = 6$ and $d = 128$. For all types of codes, CrossMPT outperforms the conventional ECCT and all the other BP-based neural decoders. This improvement of CrossMPT is particularly notable in the case of LDPC codes. To provide more visual information, we plot the BER graphs for several codes in Figure 4.

An important aspect of our research is CrossMPT's capability to decode long codes (Appendix A), which remain beyond the reach of ECCT due to its high memory requirements, resulting from large attention maps. These results demonstrate the practical significance and architectural advantages of CrossMPT, proving its value in scenarios where ECCT encounters limitations. Especially, it achieves superior decoding performance for LDPC codes, outperforming the BP decoder with the maximum iteration of 100 (provided in Appendix B). Also, we demonstrate that for short codes, CrossMPT closely approaches the optimal maximum likelihood (ML) decoding performance (provided in Appendix C). Additional experimental results for block error rate (BLER), comparison with successive cancellation list polar decoder, denoising diffusion ECCT (DDECCT), and the decoding performance for the Rayleigh channel are provided in Appendices D, E, F, and G, respectively.

6 Ablation Studies and Analysis

6.1 Analysis of Attention Mechanisms in ECCT and CrossMPT

We provide an analysis of the attention scores in ECCT and CrossMPT. Figure 5 shows the average attention scores across $N = 6$ layers for both ECCT and CrossMPT for $(32, 16)$ LDPC code (Abu-Surra et al., 2010). As shown in Figure 5, the attention score map of ECCT reveals different importance among the relationships: Magnitude-magnitude, syndrome-syndrome, and magnitude-syndrome. One key observation is that the magnitude-magnitude and syndrome-syndrome relations exhibit relatively low attention scores compared to the magnitude-syndrome relation, which suggests that the magnitude-syndrome relationship is more significant than the others. Appendix H, in which we masked the magnitude-magnitude and syndrome-syndrome relationships, revealed no significant performance difference compared to when these relationships were not masked. This demonstrates that the conventional ECCT could be enhanced by focusing on the more critical relationships, as CrossMPT achieves this by eliminating the two relations with low attention scores and concentrating solely on the magnitude-syndrome relation. Therefore, we can claim that CrossMPT more efficiently targets the crucial aspect (i.e., magnitude-syndrome relation) compared to ECCT.

6.2 Visualization of Cross-attention Map

To further examine how CrossMPT operates, we intentionally corrupt a pre-determined bit of the $(32, 16)$ LDPC code and analyze the resulting attention maps. Figure 6 shows the attention scores

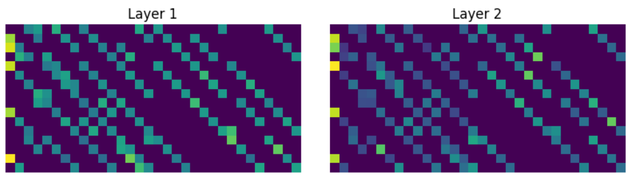

(a) Attention scores with a single bit error

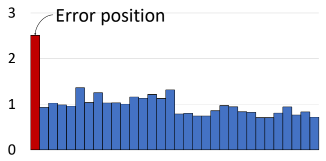

(b) Summation of attention scores with a single bit error

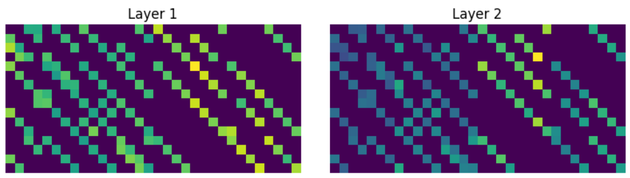

(c) Attention scores without an error

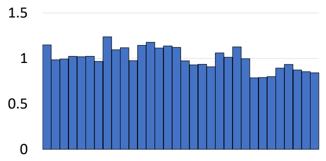

(d) Summation of attention scores without an error

Figure 6: The attention scores (a), (c) with a single bit error in the first bit position and without an error. The summation of the attention scores (b), (d) is carried out in the vertical direction.

for the first two layers and the summation of their attention scores when the *first bit* is corrupted. The summation is carried out vertically to demonstrate the attention score for each bit. As shown in Figure 6(b), the attention score of the first bit (or first column) is relatively higher than the others. However, once the error is corrected, CrossMPT no longer assigns high scores to that position (see Figure 12 in Appendix I). Figures 6(c) and 6(d) depict the attention scores and the summation of attention scores without an error. Compared to the previous case, the attention scores are more uniformly distributed across all positions.

6.3 Complexity Analysis

Two cross-attention blocks of CrossMPT share the same parameters for all decoder layers. They use the same weight matrices W_Q, W_K, W_V for two cross-attention modules since the performance remains nearly identical even when the parameters are trained separately. Also, they share the parameters for the normalization layer and the FFNN layer. Thus, CrossMPT has the same number of parameters as the original ECCT.

Figure 1 illustrates the mask matrices of ECCT and CrossMPT. In the original ECCT, Figure 1(a) shows that a significant portion of the upper $n \times n$ submatrix is depicted in white, indicating that the most positions are unmasked. This $n \times n$ submatrix represents depth-2 connections in the Tanner graph (Choukroun & Wolf, 2022a), which results in an increase in the number of unmasked positions, thereby leading to a higher computational required. On the other hand, the lower $(n - k) \times n$ submatrix and the right $(n - k) \times n$ submatrix, which serve as the masking matrices for CrossMPT, are predominantly shown in blue, indicating that their attention matrices are sparser. Figure 7 compares the mask matrix density of CrossMPT and ECCT. For all codes, the mask matrix of CrossMPT is sparser than ECCT, which implies that CrossMPT can achieve lower computational complexity compared to the original ECCT.

The complexity of the self-attention mechanism of ECCT, without considering the masking is, $\mathcal{O}(N(d^2(2n - k) + (2n - k)^2 d))$. When taking masking into account, the complexity can be reduced to $\mathcal{O}(N(d^2(2n - k) + hd))$ (Choukroun & Wolf, 2022a), where $h = \rho_1(2n - k)^2$ denotes the fixed number of computations of the self-attention module and ρ_1 denotes the density of the mask matrix in ECCT. Similarly, the complexity of the two cross-attention modules of CrossMPT, without considering the masking, is $\mathcal{O}(N(d^2(2n-k) + 2n(n-k)d))$. When masking is taken into account, the complexity can be reduced to $\mathcal{O}(N(d^2(2n-k) + (h_1 + h_2)d))$, where $h_1 = \rho_2 n(n-k)$ denotes the number of computations of the first cross-attention module, $h_2 = \rho_2(n - k)n$ denotes the number of computations of the second cross-attention module, and ρ_2 denotes the density of the mask matrix in CrossMPT. Furthermore, since $\rho_1 > \rho_2$ as shown in Figure 7, we conclude that

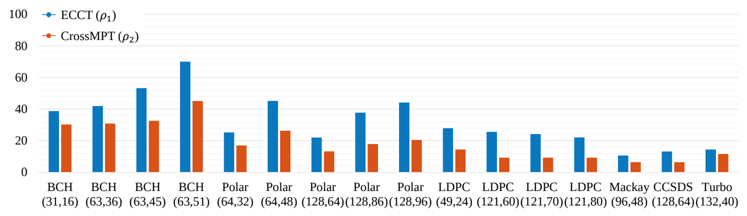

Figure 7: Comparison of the mask matrix density between ECCT and CrossMPT.

Table 2: Comparison of FLOPs, inference time, and training time between ECCT and CrossMPT for various codes. Inference time is measured for decoding a single codeword and training time is measured for a single epoch.

Codes	Parameter	FLOPs		Inference (codeword)		Training (epoch)		Mask density		Memory usage	
		CrossMPT	ECCT	CrossMPT	ECCT	CrossMPT	ECCT	CrossMPT	ECCT	CrossMPT	ECCT
BCH	(63,45)	106.4 M	99.8 M	326 μs	328 μs	29 s	29 s	32.45%	53.09%	962 MiB	1828 MiB
LDPC	(121,70)	256.8 M	229.7 M	400 μs	450 μs	58 s	80 s	9.09%	24.01%	1980 MiB	3926 MiB
	(121,80)	238.0 M	212.5 M	391 μs	436 μs	53 s	76 s	9.09%	21.94%	1936 MiB	3602 MiB
Turbo	(132,40)	343.4 M	303.6 M	459 μs	511 μs	83 s	110 s	11.43%	14.25%	2362 MiB	5580 MiB
BCH	(255,223)	53.5 M	28.2 M	747 μs	859 μs	56 s	145 s	48.63%	78.21%	1036 MiB	7318 MiB
WRAN	(384,320)	111.3 M	53.1 M	1295 μs	1638 μs	104 s	305 s	5.21%	13.25%	3270 MiB	18192 MiB

$h > h_1 + h_2$, which indicates that CrossMPT achieves a reduction in computational complexity compared the original ECCT.

Table 2 compares the total FLOPs, inference time, training time, and memory usage between ECCT and CrossMPT. The inference time refers to the duration required to decode a single codeword and the training time measures the duration to complete one epoch of training. All results are obtained for $N = 6$ and $d = 128$, except for (255,223) BCH code and (384,320) WRAN LDPC code, which are obtained for $N = 6$ and $d = 32$. For all three metrics, CrossMPT outperforms ECCT. Since the inference time and the training time are closely related to the FLOPs, a reduction in FLOPs directly leads to shorter inference and training times. Notably, CrossMPT significantly reduces memory usage compared to ECCT, especially for long codes. This improvement arises from the reduced size of the attention map; $2n(n-k)$ for CrossMPT and $(2n-k)^2$ for ECCT. The results in Tables 1 and 2 demonstrate that the proposed CrossMPT not only improves the decoding performance but also significantly reduces FLOPs, inference time, training time, and memory usage compared to the original ECCT. Additional analysis of the training time required to achieve the target loss is provided in Appendix J

CrossMPT's sequential decoding approach may limit its throughput in certain scenarios. However, pipelining (Li et al., 2021b; Rowshan et al., 2024) enables CrossMPT to effectively increase its throughput when decoding multiple codewords (see Appendix K).

7 Conclusion

We developed a novel transformer architecture for ECC decoding called CrossMPT, which improves both decoding performance and computational complexity. CrossMPT achieves this by adopting a more effective architecture that processes magnitude and syndrome through the cross-attention mechanism. This approach leverages the clear and compact representation of codeword bit relationships in the PCM, enabling the model to accurately learn these relationships while also reducing memory usage, FLOPs, inference time, and training time. Most existing research on transformer-based decoders has primarily focused on short codes due to challenges in training long codes, caused by high memory usage and complexity. However, CrossMPT offers a potential breakthrough, paving the way for transformer-based decoders to be effectively applied to long codes.

REFERENCES

A. Abu-Surra, D. DeClercq, D. Divsalar, and W. E. Ryan. Trapping set enumerators for specific LDPC codes. In *Information Theory and Applications (ITA) Workshop*, 2010.

S. K. Ankireddy and H. Kim. Interpreting neural min-sum decoders. In *IEEE International Conference on Communications (ICC)*, 2023.

J. H. Bae, A. Abotabl, H. P. Lin, KB. Song, and J. Lee. An overview of channel coding for 5G NR cellular communications. *APSIPA Transactions on Signal and Information Processing*, 8(1):e17, 2019.

A. Bennatan, Y. Choukroun, and P. Kisilev. Deep learning for decoding of linear codes-a syndrome-based approach. In *IEEE International Symposium on Information Theory (ISIT)*, pp. 1595–1599, 2018.

A. Buchberger, C. Hager, H. D. Pfister, L. Schmalen, and A. G. I. Amat. Pruning and quantizing neural belief propagation decoders. *IEEE Journal of Selected Areas in Communications*, 39(7): 1957–1966, 2021.

S. Cammerer, T. Gruber, J. Hoydis, and S. ten Brink. Scaling deep learning-based decoding of polar codes via partitioning. In *IEEE Global Communications Conference (GLOBECOM)*, 2017.

N. Carion, F. Massa, G. Synnaeve, N. Usunier, A. Kirillov, and S. Zagoruyko. End-to-end object detection with transformers. In *European Conference on Computer Vision (ECCV)*, 2020.

C.-F. Chen, Q. Fan, and R. Panda. CrossViT: Cross-attention multi-scale vision transformer for image classification. In *IEEE/CVF International Conference on Computer Vision (ICCV)*, 2021.

Y. Choukroun and L. Wolf. Error correction code transformer. In *Advances in Neural Information Processing Systems (NeurIPS)*, 2022a.

Y. Choukroun and L. Wolf. Error correction code transformer. `https://github.com/yoniLc/ECCT`, 2022b. Accessed: 2023-05-22.

Y. Choukroun and L. Wolf. Denoising diffusion error correction codes. In *International Conference on Learning Representations (ICLR)*, 2023.

Y. Choukroun and L. Wolf. A foundation model for error correction codes. In *International Conference on Learning Representations (ICLR)*, 2024a.

Y. Choukroun and L. Wolf. Learning linear block error correction codes. In *International Conference on Machine Learning (ICML)*, 2024b.

J. Dai, K. Tan, Z. Si, K. Niu, M. Chen, H. V. Poor, and S. Cui. Learning to decode protograph LDPC codes. *IEEE Journal of Selected Areas in Communications*, 39(7):1983–1999, 2021.

J. Devlin, M.-W. Chang, K. Lee, and K. Toutanova. BERT: Pre-training of deep bidirectional transformers for language understanding. In *North American Chapter of the Association for Computational Linguistics (NAACL)*, 2019.

M. P. C. Fossorier, M. Mihaljevic, and H. Imai. Reduced complexity iterative decoding of low-density parity check codes based on belief propagation. *IEEE Transactions on Communications*, 47(5):673–680, 1999.

R. Girshick, J. Donahue, T. Darrell, and J. Malik. Rich feature hierarchies for accurate object detection and semantic segmentation. In *IEEE/CVF Conference on Computer Vision and Pattern Recognition (CVPR)*, 2014.

T. Gruber, S. Cammerer, J. Hoydis, and T. Brink. On deep learning-based channel decoding. In *51st Annual Conference on Information Sciences and Systems (CISS)*, pp. 1–6, 2017.

P. Hailes, L. Xu, R. G. Maunder, B. M. Al-Hashimi, and L. Hanzo. A survey of FPGA-based LDPC decodes. *IEEE Communications Surveys & Tutorials*, 18(2):1098–1122, 2015.

K. He, X. Zhang, S. Ren, and J. Sun. Deep residual learning for image recognition. In *IEEE/CVF Conference on Computer Vision and Pattern Recognition (CVPR)*, 2016.

M. Helmling, S. Scholl, F. Gensheimer, T. Dietz, D. Kraft, S. Ruzika, and N. Wehn. Database of Channel Codes and ML Simulation Results. In `https://rptu.de/en/channel-codes`, 2019.

H. Kim, Y. Jiang, R. Rana, S. Kannan, S. Oh, and P. Viswanath. Communication algorithms via deep learning. In *International Conference on Learning Representations (ICLR)*, 2018.

H. Kim, S. Oh, and P. Viswanath. Physical layer communication via deep learning. *IEEE Journal of Selected Topics in Information Theory*, 1(1):5–18, 2020.

D. P. Kingma and J. Ba. Adam: A method for stochastic optimization. In *International Conference on Learning Representations (ICLR)*, 2015.

H.-Y. Kwak, J.-W. Kim, Y. Kim, S.-H. Kim, and J.-S. No. Neural min-sum decoding for generalized LDPC codes. *IEEE Communications Letters*, 26(12):2841–2845, 2022.

H.-Y. Kwak, D.-Y. Yun, Y. Kim, S.-H. Kim, and J.-S. No. Boosting Learning for LDPC Codes to improve the error-floor performance. In *Advances in Neural Information Processing Systems (NeurIPS)*, 2023.

F. Li, C. Zhang, K. Peng, A. E. Krylov, A. A. Katyushnyj, A. V. Rashich, D. A. Tkachenko, S. B. Makarov, and J. Song. Review on 5G NR LDPC code: Recommendations for DTTB system. *IEEE Access*, 9:155413–155424, 2021a.

M. Li, V. Derudder, K. Bertrand, C. Desset, and A. Bourdoux. High-speed LDPC decoders towards 1 Tb/s. *IEEE Transactions on Circuits and Systems I: Regular Papers*, 68(5):2224–2233, 2021b.

L. Lugosch and W. J. Gross. Neural offset min-sum decoding. In *IEEE International Symposium on Information Theory (ISIT)*, pp. 1316–1365, 2017.

E. Nachmani and L. Wolf. Hyper-graph-network decoders for block codes. In *Advances in Neural Information Processing Systems (NeurIPS)*, pp. 2326–2336, 2019.

E. Nachmani and L. Wolf. Autoregressive belief propagation for decoding block codes. *arXiv preprint arXiv:2103.11780*, 2021.

E. Nachmani, Y. Beery, and D. Burshtein. Learning to decode linear codes using deep learning. In *54th Annual Allerton Conference on Communications, Control, and Computing (Allerton)*, pp. 341–346, 2016.

E. Nachmani, E. Marciano, L. Lugosch, W. J. Gross, D. Burshtein, and Y. Beery. Deep learning methods for improved decoding of linear codes. *IEEE Journal of Selected Topics in Signal Processing*, 12(1):119–131, 2018.

S.-J. Park, H.-Y. Kwak, S.-H. Kim, S. Kim, Y. Kim, and J.-S. No. How to mask in error correction code transformer: Systematic and double masking. In *arXiv preprint arXiv:2308.08128*, 2023.

T. Richardson and R. Urbanke. The capacity of low-density parity check codes under message-passing decoding. *IEEE Transactions on Information Theory*, 47(2):599–618, 2001.

R. Rombach, A. Blattmann, D. Lorenz, P. Esser, and B. Ommer. High-resolution image synthesis with latent diffusion models. In *IEEE/CVF Conference on Computer Vision and Pattern Recognition (CVPR)*, 2022.

M. Rowshan, M. Qiu, Y. Xie, X. Gu, and J. Yuan. Channel coding toward 6G: Technical overview and outlook. *IEEE Open Journal of the Communications Society*, 5:2585–2685, 2024.

A. Vaswani, N. Shazeer, N. Parmar, J. Uszkoreit, L. Jones, A. N. Gomez, Ł. Kaiser, and I. Polosukhin. Attention is all you need. In *Advances in Neural Information Processing Systems (NeurIPS)*, 2017.

L. Wang, S. Chen, J. Nguyen, D. Dariush, and R. Wesel. Neural-network-optimized degree-specific weights for LDPC minsum decoding. In *IEEE International Symposium on Topics in Coding (ISTC)*, 2021.

A Performance on Longer Codes

We present the BER performance for three longer codes in Figures 8(a), 8(b), and 8(c) for ECCT and CrossMPT $N = 6$, $d = 32$. For all three codes ((a) (529,440) LDPC code, (b) (384,320) wireless regional area network (WRAN) LDPC code, (c) (512,384) polar code), the proposed CrossMPT outperforms the original ECCT. Despite its reduced complexity, CrossMPT significantly enhances the decoding performance compared to ECCT, not only for short-length codes but also for longer codes. Also, Figures 8(d) and 8(e) show the decoding performance of CrossMPT for much longer codes. The BER performances of the (648,540) IEEE802.11n LDPC code ($N = 10$, $d = 128$) and (1056,880) WiMAX LDPC code ($N = 6$, $d = 32$) demonstrate that CrossMPT efficiently trains how to decode the codeword even for large N and d and performs well for longer codes. Again, we emphasize CrossMPT's capability to decode long codes where ECCT struggles due to high memory allocation (large attention map). The structure of CrossMPT demonstrates its efficiency in learning long codes, surpassing the limitations of short or moderate codelengths of transformer-based decoders.

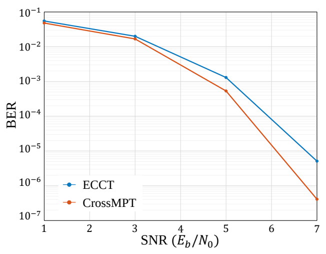

(a) (529,440) LDPC code

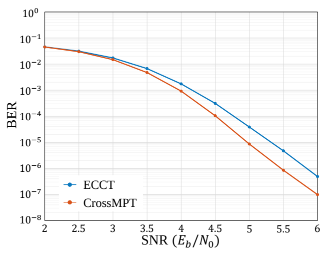

(b) (384,320) WRAN LDPC code

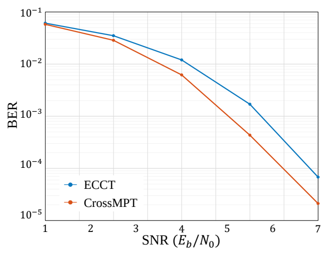

(c) (512,384) polar code

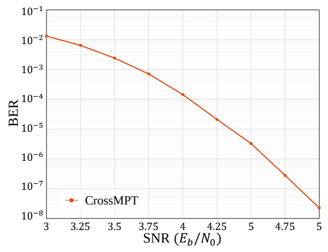

(d) (648,540) IEEE802.11n

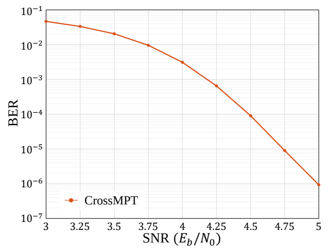

(e) (1056,880) WiMAX

Figure 8: The decoding performance of long codes.

B Comparison with the BP decoder

Figure 9 shows the decoding performance between the traditional BP decoder with a maximum number of iterations of 20, 50, and 100 and CrossMPT for both short and long LDPC codes. Figures 9(a) and 9(b) compare the BER performance for (121,80) LDPC codes ($N = 6$, $d = 128$) and (648,540) IEEE 802.11n LDPC code ($N = 10$, $d = 128$), respectively. Notably, the proposed CrossMPT can outperform the BP decoder for both short and long LDPC codes. These results highlight that CrossMPT efficiently trains how to decode the codeword across a wide range of code lengths.

C Comparison with the ML decoder

We compare ECCT and CrossMPT with the ML decoder for short BCH codes. Figure 9 demonstrates the BER performance of $(31, 16)$ BCH code and $(31, 21)$ BCH code. Especially, these results show that CrossMPT closely approaches the optimal ML performance for short codes.

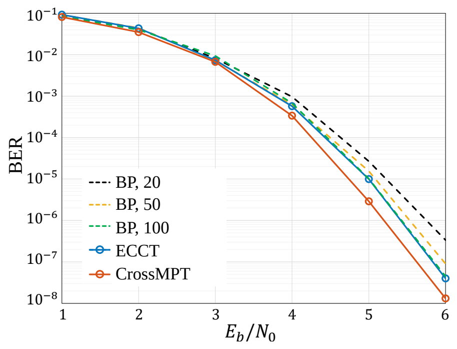

(a) (121,80) LDPC code

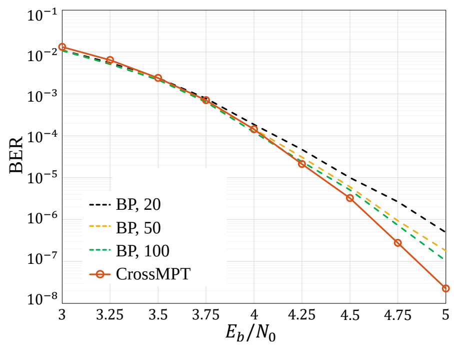

(b) (648,540) IEEE 802.11n

Figure 9: Performance comparison between BP decoder (iteration 20, 50, and 100) and CrossMPT.

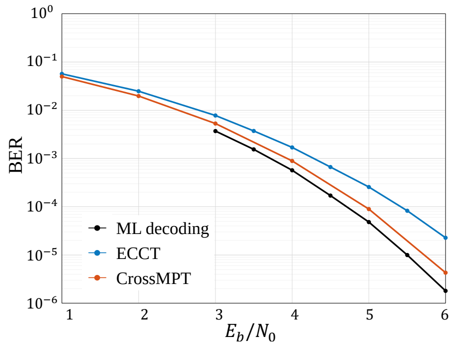

(a) (31,16) BCH code

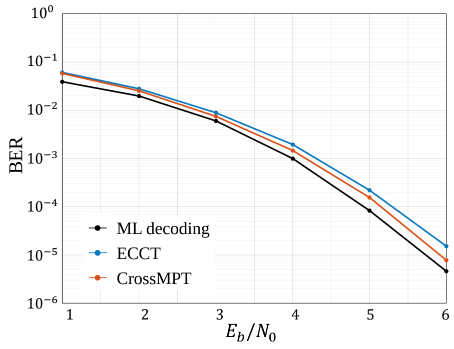

(b) (31,21) BCH code

Figure 10: The decoding performance comparison between ML decoder, ECCT, and CrossMPT.

D Block Error Rate Performance

Table 3 demonstrates BLER results for various code classes ($N = 6, d = 128$). Also, Figure 11 shows the BLER performance of (31,16) BCH code, (63,51) BCH code, and (648,540) IEEE 802.11n LDPC code. For BCH codes, we compare the decoding performance of CrossMPT with the traditional Berlekamp-Massey (BM) decoder, maximum liklihood (ML) decoding algorithm, ECCT. For LDPC codes, we compare the decoding performance of CrossMPT with the traditional BP decoder with a maximum number of iterations of 20, 50, and 100. As shown in the table, CrossMPT outperforms ECCT in BLER performance and also has a comparable BLER results compared to the traditional decoding algorithms.

In addition, the traditional decoders are code-specific decoders, tailored to each class of codes. For example, LDPC codes are effectively decoded by the BP decoder, BCH codes by the BM decoder, and polar codes by the SCL decoder. However, unlike the traditional decoders, a key advantage of CrossMPT is its versatility. While conventional decoders are good and valid only for respective code classes, CrossMPT performs effectively across a wide range of code classes. This universality highlights the broader applicability and potential of CrossMPT in various decoding scenarios and future communication paradigm such and semantic communication.

The complexity of transformer-based decoders is relatively high compared to code-specific decoders. Reducing their computational requirements will be an important focus for future work.

Table 3: The BLER results for ECCT and CrossMPT. The results are measured by the negative natural logarithm of BLER.

Method	ECCT			CrossMPT		
SNR	4	5	6	4	5	6
(31,16) BCH	4.19	5.98	8.16	5.12	7.24	10.31
(63,36) BCH	2.43	4.10	6.40	2.50	4.23	6.61
(63,45) BCH	2.75	4.75	7.67	3.18	5.33	8.66
(63,51) BCH	2.72	4.85	7.82	2.94	5.16	8.36
(64,32) Polar	4.18	6.47	9.07	4.83	7.26	10.41
(64,48) Polar	3.08	5.06	7.60	3.56	5.68	8.35
(49,24) LDPC	3.62	5.89	9.39	4.47	7.20	10.68
(121,70) LDPC	3.21	6.69	11.91	4.28	8.42	13.35

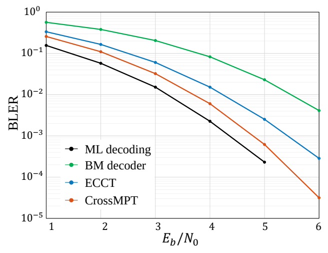

(a) (31,16) BCH code

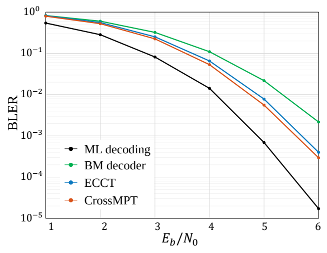

(b) (63,51) BCH code

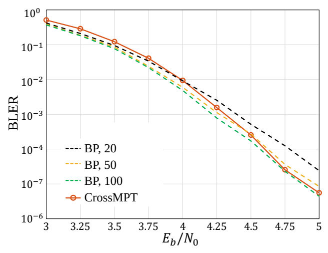

(c) (648,540) IEEE 802.11n

Figure 11: The BLER performance comparison between the traditional decoders and CrossMPT.

E Comparison with Successive Cancellation List Polar Decoder

We compare the BER performance of the SCL decoder, ECCT, and CrossMPT in Table 4. The performance of the SCL decoder is from (Choukroun & Wolf, 2022a). Although the contribution of L is significant in long codes, the SCL decoder achieves a great performance with small L, such as $L = 4$. As reported in (Choukroun & Wolf, 2022a; 2023), the SCL decoder outperforms ECCT. This is because the SCL decoder is a decoder specialized for Polar codes and is a state-of-the-art algorithm that has undergone extensive development over a long period. CrossMPT has made significant improvements from ECCT and even outperforms the SCL decoder for (64,48) polar code.

Table 4: Comparison of decoding performance at three different SNR values (4 dB, 5 dB, 6 dB) for SCL decoder, ECCT, and CrossMPT. The results are measured by the negative natural logarithm of BER. The best results are highlighted in **bold** and the second best is underlined. Higher is better.

Method	SCL ($L = 1$)			SCL ($L = 4$)			ECCT			CrossMPT		
Parameter	4	5	6	4	5	6	4	5	6	4	5	6
(64,32)	7.30	9.67	13.18	**8.11**	**10.70**	**14.04**	6.99	9.44	12.32	7.50	9.97	13.31
(64,48)	6.19	8.41	10.97	**6.69**	8.63	11.24	6.36	8.46	11.09	6.51	**8.70**	**11.31**
(128,64)	8.37	11.69	13.70	**9.60**	**13.16**	**17.42**	5.92	8.64	12.18	7.52	11.21	14.76
(128,86)	7.54	10.74	15.14	**9.26**	**13.04**	**17.13**	6.31	9.01	12.45	7.86	11.45	15.47
(128,96)	6.74	9.53	13.53	**8.02**	**11.60**	**18.16**	6.31	9.12	12.47	7.15	10.15	13.13

F Comparison with DDECCT

For a fair comparison with DDECCT, we also apply the denoising diffusion training technique to CrossMPT. Table 5 compares the BER performance of ECCT (Choukroun & Wolf, 2022a), CrossMPT, DDECCT, and CrossMPT applying the denoising diffusion model. All four decoders are model-free decoders using the transformer architecture, and simulations are taken for $N = 6$,

$d = 128$. We conduct simulations for codes where DDECC performs better than CrossMPT. For the rest of the codes, CrossMPT outperforms DDECC. The proposed CrossMPT shows superior decoding performance compared to the original ECCT. Compared to DDECC, CrossMPT demonstrates similar BER performance for polar codes, but it even outperforms DDECC for BCH and LDPC codes. When the denoising diffusion technique is applied to CrossMPT, it achieves the best performance among others, where DDECC, CrossMPT, and ECCT follow. This proves that the CrossMPT architecture provides separate gain from the denoising diffusion algorithm for transformer-based decoders.

Table 5: Comparison of decoding performance at three different SNR values (4 dB, 5 dB, 6 dB) for ECCT (Choukroun & Wolf, 2022a), CrossMPT, and DDECC (Choukroun & Wolf, 2023). The results are measured by the negative natural logarithm of BER. The best results are highlighted in **bold** and the second best is underlined. Higher is better.

Architecture		*Without* denoising diffusion						*With* denoising diffusion					
Codes	Parameter	ECCT			CrossMPT			ECCT			CrossMPT		
		4	5	6	4	5	6	4	5	6	4	5	6
BCH	(63,36)	4.86	6.65	9.10	5.03	6.91	9.37	5.11	7.09	9.82	**5.23**	**7.20**	**10.01**
Polar	(128,64)	5.92	8.64	12.18	7.52	11.21	14.76	9.11	12.9	16.30	**10.21**	**13.63**	**17.28**
	(128,86)	6.31	9.01	12.45	7.51	10.83	15.24	7.60	10.81	15.17	**8.56**	**12.04**	**15.37**
	(128,96)	6.31	9.12	12.47	7.15	10.15	13.13	7.16	10.3	13.19	**7.57**	**10.61**	**13.33**
MacKay	(96,48)	7.38	10.72	14.83	7.97	11.77	15.52	8.12	11.88	15.93	**8.85**	**12.58**	**17.69**

G Decoding Performance for Rayleigh Fading Channel

The original ECCT architecture shows robustness to non-Gaussian channels (e.g., Rayleigh fading channel) (Choukroun & Wolf, 2022a, Supplementary). We also measured the decoding performance of CrossMPT in Rayleigh fading channels. To compare with ECCT, we use the same fading channel as in (Choukroun & Wolf, 2022a). The received codeword is given as $y = hx + z$, where h is an n-dimensional i.i.d. Rayleigh distributed vector with a scale parameter $\alpha = 1$ and $z \sim N(0, \sigma^2)$. The following table demonstrates the BER performance of ECCT and CrossMPT in Rayleigh fading channel and CrossMPT still outperforms the original ECCT architecture for all types of codes.

Codes	(31,16) BCH			(64,32) Polar			(128,64) Polar			(128,86) Polar			(121,70) LDPC			(128,64) CCSDS		
Methods	4	5	6	4	5	6	4	5	6	4	5	6	4	5	6	4	5	6
ECCT	5.18	6.04	6.92	5.53	6.62	7.80	4.31	5.37	6.63	4.02	4.81	5.70	3.91	4.97	6.31	2.46	3.97	5.79
CrossMPT	5.53	6.55	7.61	5.91	7.17	8.48	4.70	5.93	7.34	4.41	5.38	6.46	4.25	5.53	7.11	5.25	6.94	8.92

H Ablation Study with Additional Masking

To understand the impact of magnitude-magnitude and syndrome-syndrome relationships, we exammine the decoding performance of ECCT with additional masking applied to all positions corresponding to these relationships. Table 6 compares the decoding performance of ECCT with this additional masking, standard ECCT, and CrossMPT. The results show no significant performance degradation with the additional masking, indicating that the magnitude-magnitude and syndrome-syndrome relationships are not critical to decoding performance.

I Visualization of Cross-Attention Map

Figure 12 illustrates the attention scores for all $N = 6$ layers with a single bit error (bit error in the *first position*). The first three layers have relatively high attention score at the error position (first bit). Then, when the error is corrected, the attention score becomes lower at the last three layers.

Table 6: Comparison of decoding performance at three different SNR values (4 dB, 5 dB, 6 dB) for ECCT with additional masking, standard ECCT, and CrossMPT. The results are measured by the negative natural logarithm of BER. The best results are highlighted in **bold**. Higher is better.

Method	ECCT + Masking			ECCT			CrossMPT		
Parameter	4	5	6	4	5	6	4	5	6
$(31, 16)$ BCH	6.52	8.55	11.42	6.39	8.29	10.66	**6.98**	**9.25**	**12.48**
$(63, 45)$ BCH	5.53	7.74	10.88	5.60	7.79	10.93	**5.90**	**8.20**	**11.62**
$(64, 48)$ Polar	6.25	8.26	10.93	6.36	8.46	11.09	**6.51**	**8.70**	**11.31**
$(121, 60)$ LDPC	4.98	7.91	12.61	5.17	8.31	13.30	**5.74**	**9.26**	**14.78**

For model-based neural decoders, interpretation and analysis in terms of graphs are feasible because their structural architecture is inherently based on conventional graph-based decoding algorithms (Wang et al., 2021; Ankireddy & Kim, 2023). However, in the case of model-free approaches, it remains challenging to determine how attention scores or weights are assigned to specific nodes and how these assignments are influenced by graph properties such as node degree.

Although we analyzed how the attention scores change depending on where the error occurs in Figure 12, we have not yet achieved a rigorous analysis beyond this level. This remains a critical issue in model-free approaches and represents a problem that needs to be addressed in future work.

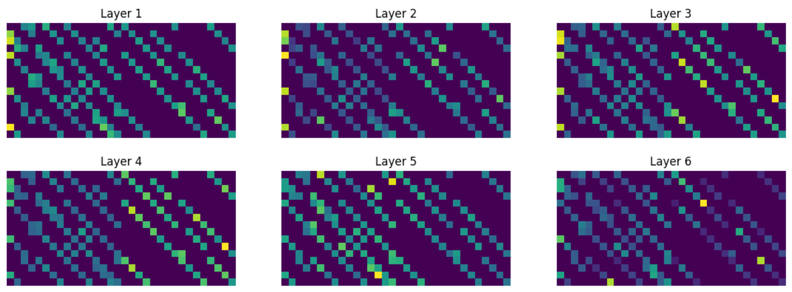

Figure 12: Attention scores of $N = 6$ layers with a single bit error.

J Training Time to Achieve the Target Loss

In Table 7, we compare the training time required for ECCT and CrossMPT to achieve the target loss. The target loss is set as a minimum loss of ECCT during the training. For $(128, 86)$ polar code, the minimum loss of ECCT during the 1000 epochs is 2.28×10^{-2}. To achieve the loss 2.28×10^{-2}, CrossMPT takes 6912 s, while ECCT requires 72917 s. Similarly, for $(128, 64)$ CCSDS code, the minimum loss of ECCT is 2.79×10^{-2} and CrossMPT requires 2356 s, while ECCT requires 85770 s. These results demonstrate that CrossMPT achieves the target loss significantly faster than ECCT, highlighting its efficiency in terms of training time.

Table 7: Comparison of training time to achieve the target loss for ECCT and CrossMPT.

Codes	Methods	Target loss	Time
(128,86) Polar	ECCT	2.28×10^{-2}	72917 s
	CrossMPT	2.28×10^{-2}	6912 s
(128,64) CCSDS	ECCT	2.79×10^{-2}	86770 s
	CrossMPT	2.79×10^{-2}	2356 s

K Throughput Analysis

Table 2 demonstrates that CrossMPT outperforms ECCT in terms of inference time. However, while a fully parallel processor can accelerate ECCT, the sequential decoding architecture of CrossMPT limits its potential for throughput improvement. To address this, a pipelining approach—commonly employed in various ECC decoders (Li et al., 2021b; Rowshan et al., 2024)—can be applied to maximize CrossMPT's decoding throughput (see Figure 3 in (Li et al., 2021b)). By unrolling two cross-attention blocks, CrossMPT can simultaneously process two consecutive codewords across two cross-attention blocks within the same layer. This means that while the second cross-attention block processes the first codeword, the first cross-attention block concurrently decodes the subsequent codeword. This pipelining strategy ensures that CrossMPT maintains speed advantages over ECCT, in fully parallel scenarios. Figure 13 provides an example of decoding multiple codewords in CrossMPT with $N = 2$.

In wireless communications, the decoder's throughput is often a more critical concern than latency. This is because the latency from communication protocols and signal processing in preceding receiver blocks would be longer than the latency introduced by the channel decoder. Throughput becomes especially important when supporting very high data rates in wireless communication as the channel decoder can be a bottleneck.

Furthermore, in wireless communication scenarios, a sequential algorithm may be preferred for its enhanced performance or reduced complexity. The layered decoding algorithm for LDPC codes has been widely adopted as a de facto standard (Bae et al., 2019; Hailes et al., 2015; Li et al., 2021a), despite its sequential nature and limitation on parallelism, exemplifying the preference for sequential algorithms. The layered decoding algorithm is favored for its superior decoding performance compared to fully parallel sum-product decoding at equivalent computational complexities.

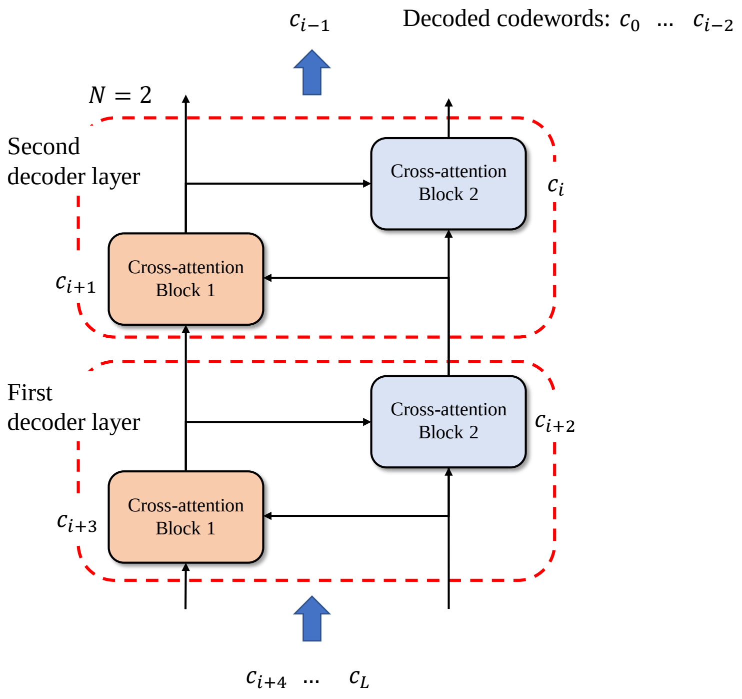

Figure 13: Example of decoding multiple codewords in CrossMPT with $N = 2$.